AAS 17-323

B-PLANE EVOLUTION UNDER HIGHLY NON-KEPLERIAN DYNAMICS

Yu Takahashi[*], Davide Farnocchia[*], Paul Thompson[*], Nicholas Bradley[*], Shadan Ardalan[†], John Bordi[‡]

Juno is the second of a series of New Frontiers missions and was launched in 2011. The spacecraft was set en route to Jupiter, and its Jupiter Orbit Insertion occurred on 2016-07-04 after a five-year cruise in deep space. The mission phase just prior to this large maneuver is called approach. As navigation team, we were responsible for precise orbit determination of the Juno spacecraft to ensure a successful orbit insertion. To evaluate the navigation performance we employed the B-plane mapping, where the incoming hyperbolic velocity defines the plane perpendicular to it, and the time to go to hit the plane will directly map into the uncertainties of the target point. The B-plane is a convenient tool when assessing the navigation performance as it is not affected by non-linearities due to the gravitational pull of the targeted body. However, as the Jupiter Orbit Insertion approached we started to realize that the B-plane mapping uncertainties were significantly larger than expected. We found that the B-plane mapping time had tremendous influence on the covariance inflation in the B-plane. Because of the close approach distance during the Jupiter Orbit Insertion and the strong interaction with J_2 spherical harmonic coefficient, the Juno dynamics were too far from a Keplerian one assumed for the B-plane mapping. We first discuss the analytical approach of the B-plane mapping uncertainty and perform a numerical analysis to isolate the components of the Juno dynamics that cause the B-plane covariance inflation.

INTRODUCTION

Launched on 2011-08-05 from Cape Canaveral on an Atlas V, Juno is the second of a series of New Frontiers missions. The spacecraft was set en route to Jupiter after a couple of deep space maneuvers and an Earth flyby in October 2013. After a five-year cruise in deep space, the Jupiter Orbit Insertion (JOI) occurred on 2016-07-04. The JOI maneuver put Juno in a 53.5-day orbit.

The Juno navigation team is at the Jet Propulsion Laboratory (JPL) and consists of three teams: orbit determination (OD), maneuver design (MD), and trajectory design. The OD team estimates the Juno trajectory (position and velocity as a function of time) and other pertinent dynamical forces (e.g., maneuvers, solar radiation pressure, turns from the attitude control, etc). The MD team designs the maneuvers to put the spacecraft back on the reference trajectory based on the state of the spacecraft as estimated by the OD. The trajectory design team designs the reference trajectory that serves as the nominal mission profile for the entire mission. This manuscript is focused on the

[*]Orbit Determination Analyst, Mission Design and Navigation Section, Jet Propulsion Laboratory, California Institute of Technology, 4800 Oak Grove Drive, CA 91109

[†]Juno Orbit Determination Team Lead, Mission Design and Navigation Section, Jet Propulsion Laboratory, California Institute of Technology, 4800 Oak Grove Drive, CA 91109

[‡]Juno Navigation Team Lead, Mission Design and Navigation Section, Jet Propulsion Laboratory, California Institute of Technology, 4800 Oak Grove Drive, CA 91109

approach phase just prior to JOI, and how the OD team navigated the spacecraft and their performance. Table 1 lists the nominal schedule of the trajectory correction maneuvers (TCMs) since the beginning of 2016.

Table 1. Juno Maneuver Schedule before JOI.

Date	Maneuver	Type	Status
2016-02-03	TCM-11	Deterministic	Executed
2016-04-13	Crosses the sphere of influence of Jupiter		
2016-05-31	TCM-12	Statistical	Cancelled
2016-06-15	TCM-12a	Statistical (contingency for TCM-12)	Cancelled
2016-06-25	TCM-13	Statistical (second contingency for TCM-12)	Cancelled

All but one maneuver, namely TCM-11, were cancelled because of good maneuver execution performance and stability of the OD solutions. The final OD solution used to design JOI was delivered on 2016-02-22, after the execution of TCM-11. Thus, that OD solution, named OD133, became the de facto reference target for the subsequent OD solution deliveries.

Traditionally, the B-plane is computed by taking the predicted spacecraft state at the time of close approach and constructing a Keplerian trajectory backward in time. For Juno, the closest approach occurs at the perijove of the trajectory without the JOI maneuver in the model. As we approached the JOI maneuver, we noticed that the uncertainty associated with the B-plane parameters did not match our intuition and was unreasonably large for all considered perturbation sources. It is the purpose of this paper to discuss how we identified and resolved the problem prior to the JOI execution.

B-PLANE DEFINITION

The B-plane is a concept often used in interplanetary navigation[1] and asteroid hazard assessment.[2] It is a convenient set of coordinates that is not affected by the non-linear dynamics and mapping of the spacecraft state relative to the target body. Figure 1 shows the geometry of the B-plane relative to the incoming hyperbolic spacecraft trajectory.

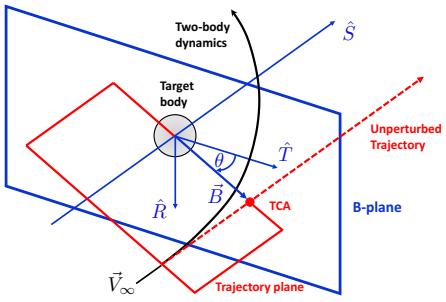

Figure 1. B-plane Geometry.

In Figure 1, $\vec{V}_\infty$ is the incoming hyperbolic velocity, which defines the B-plane oriented perpendicular to it. The coordinate frame is defined by the orthonormal vectors $\hat{R}$, $\hat{S}$, and $\hat{T}$. $\hat{S}$ is defined along $\vec{V}_\infty$, and $\hat{T}$ lies along the cross product of $\hat{S}$ and the z-component of EME2000 (i.e., in-plane

with Earth's mean equator). Then, $\hat{R}$ completes the right-hand system. The spacecraft trajectory in black represents a snapshot of the spacecraft state at particular epoch, with the Keplerian dynamics applied before and after the chosen epoch. That is, the spacecraft is propagated with Keplerian dynamics and all other perturbations are neglected.

If there was no primary body, which in our case is Jupiter, the spacecraft will continue on the dashed red line with the time of closest approach (TCA) occurring at the intersection with the B-plane. However, with the presence of the gravitational field of the primary body, the spacecraft trajectory bends and deviates from the asymptote. Thus, the spacecraft trajectory shown in black and the unperturbed trajectory in red are different and cross the B-plane at different locations and times.

The B-plane defines $\vec{B}$ as the vector from the primary body to the intersection of the asymptote with the B-plane. The angle θ is measured from $\vec{T}$ to $\vec{B}$. The B-plane parameters are conventionally expressed with $\vec{B} \cdot \hat{R} = \mathbf{B} \cdot \mathbf{R} = B \sin\theta$, $\vec{B} \cdot \hat{T} = \mathbf{B} \cdot \mathbf{T} = B \cos\theta$, and TCA. This representation of the spacecraft trajectory is useful because the change in the B-plane is unaffected by non-linearities due to the gravitational attraction of the primary body. For later use, we present the magnitude of $\vec{B}$ below:

$$|\vec{B}| \quad = \quad B \quad = r_p \sqrt{1 + \frac{V_e^2}{V_\infty^2}} \quad = \quad r_p \sqrt{1+h} \tag{1}$$

$$V_e \quad = \quad \sqrt{\frac{2GM}{r_p}} \tag{2}$$

$$h \quad = \quad \frac{V_e^2}{V_\infty^2} \tag{3}$$

where r_p is the periapsis radius, and V_e is the escape velocity. Since Juno is approaching Jupiter from the pole, $\vec{B}$ is almost along the negative $\hat{R}$ direction and θ is close to $-90°$.

FILTER SET-UP AND MAPPED UNCERTAINTY

Spacecraft orbit determination is a least squares estimation process which minimizes the discrepancy between the observed values of the data compared against predicted values based on a model. Briefly, the model includes the dynamics of the spacecraft and other perturbing forces as well as any environmental effect that affects the data (e.g., troposphere and ionosphere calibrations). The discrepancy between the observed and expected data indicates how offset the modeled parameters are from the truth, within the limitations of the adopted model. The parameters that affect the dynamics or measurements can be estimated or "considered" (the parameter contributes to the uncertainty but is not adjusted), and the machinery to perform the least-squares estimation is often referred to as a filter.[3,4] We only present its overview here, and the detailed filter setup for the Juno project is explained by Thompson et al.[5] Table 2 shows the list of estimated and considered parameters in our filter setup.

Table 2. Juno Filter Setup. The starred parameters in the baseline consider parameter list are estimated in certain sub-cases.

Acting forces
Sun and planetary gravity fields
Jupiter's harmonic gravity (J_2, J_4, and J_6)
Jupiter moons' gravity (four Galilean moons and Amalthea)
Solar radiation pressure (SRP)
Small forces (SFF)
Maneuvers

Estimated parameters (baseline)
Juno position and velocity (Sun-centered or Jupiter baycenter-centered)
SRP scaling factor
SFF
Maneuvers

Considered parameters (baseline)
Jupiter barycenter ephemeris* (DE434)
Jupiter satellite parameters (JUP310)
- Jupiter barycenter GM*
- Jupiter's zonal harmonics* (J_2, J_4, and J_6)
- Jupiter's pole (right ascension and declination)
- Jupiter moons' ephemeris
- Jupiter moons' GMs
Deep Space Network Station Locations
Troposphere and Ionosphere calibration
Earth Orientation Parameter
Quasar Locations

In Table 2, DE434[6] is the designation of planetary and lunar ephemerides used by Juno in the approach phase. The Jupiter satellite trajectory used was the JUP310 file and its covariance includes, in addition to the satellites' orbits, the GMs, Jupiter's zonal harmonics, and Jupiter's pole orientation. The uncertainties of these satellite parameters are all correlated; thus, when they are considered in the filter, they must all be included together. When a subcomponent of the correlated parameters are moved to the estimated list, the remaining Jupiter satellite parameters are no longer considered and removed from the filter. Only the estimated parameters are redefined as the nominal together with a priori covariance. The small forces are commonly used terminology at JPL to refer to thruster firings for attitude control purposes. They occur at an average of every few days to keep the high-gain antenna (HGA) pointed toward the Earth within 0.3°. The processed data types are Doppler, ranging, and Delta Differential One-way Range (DDOR), an angular measurement of the spacecraft position in the plane-of-sky calibrated by quasars.

Figure 2 shows the B-plane mapping with the latest data cut off (DCO) of 2016-05-09 for OD139.

The mapped time is the periapsis time for a no-JOI trajectory, which occurs around 02:48 ET, 2016-07-05. ET is the ephemeris time and is identical to Dynamical Barycentric Time (TDB).

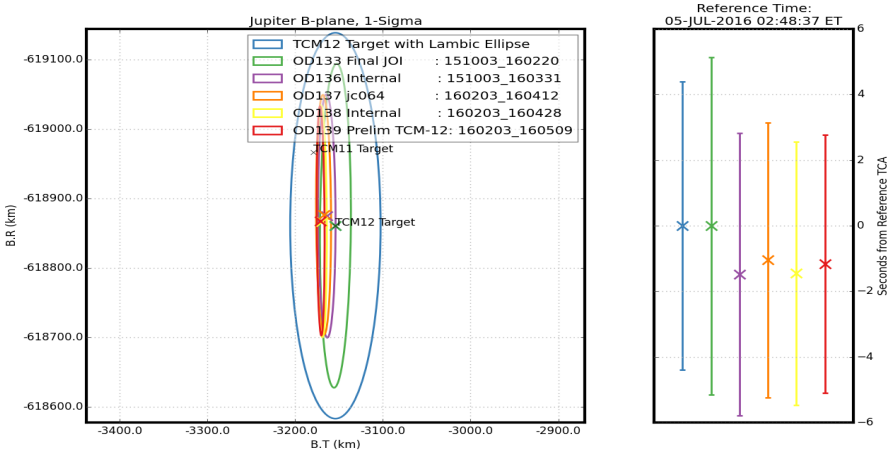

(a) B-plane plots

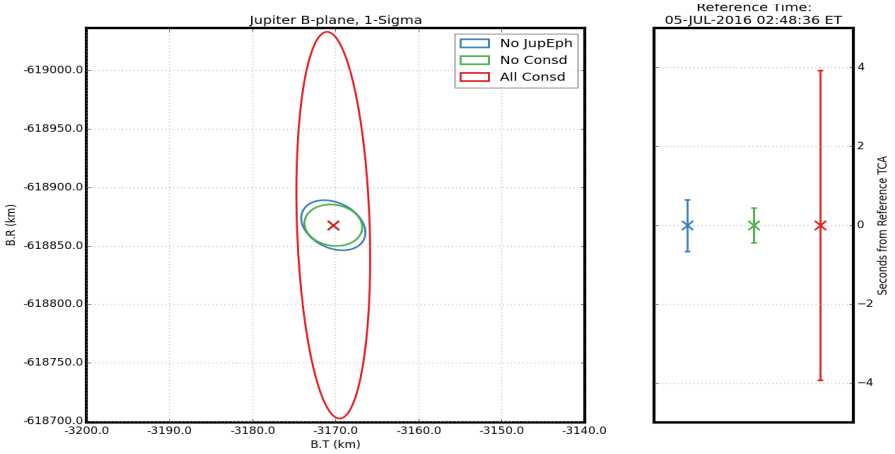

(b) OD139 consider parameter sensitivity

Figure 2. B-plane mappings for OD139 (DCO: 2016-05-09). The map time is the periapsis time without the JOI. The OD number is incremented by one for each solution delivery. OD133 is used for the final JOI design. OD136 and OD138 are the internal OD deliveries to check the solution stability. OD137 is used for jc064 background sequence design. OD139 is the preliminary OD delivery for the TCM-12. For each maneuver design, there are always two solution deliveries of preliminary and final.

Figure 2(a) shows the target points on the B-plane and the evolution of the OD solutions. Each solution label indicates the purpose of the solution delivery and the data arc in YYMMDD notation. For example, OD133 spans 2015-10-03 to 2016-02-20, and was used to design the JOI maneuver. The $\mathbf{B} \cdot \mathbf{R}$ and $\mathbf{B} \cdot \mathbf{T}$ predictions and associated error ellipses are shown on the left panel, while the TCA estimates and uncertainties are shown on the right one. The target points show where TCM-11 and TCM-12 are targeting, respectively. The predicted TCM-12 execution error ellipse is shown in blue.

Figure 2(b) shows a subset of the sensitivity analysis to the B-plane mapping. All data types are used for each case (i.e., Doppler, ranging, and DDOR). The red error ellipse is for the baseline

case with all consider parameters. The blue ellipse removes the Jupiter barycenter ephemeris from the consider list but keeps all others. The green error ellipse removes all consider parameters, so the error sources are due to the mapping of the estimated parameters (i.e., spacecraft dynamics, SFF, and SRP) as well as future small force predictions. This figure shows that the OD uncertainty is dominated by the Jupiter barycenter ephemeris (JBE), which inflates the $\mathbf{B} \cdot \mathbf{R}$ uncertainty to approximately 165 km. The actual values of the B-plane uncertainty are shown in Table 3.

Table 3. B-plane mapping uncertainties for OD139.

Case	$\sigma_{B \cdot R}\ [km]$	$\sigma_{B \cdot T}\ [km]$	$\sigma_{TCA}\ [s]$
All consider parameters	165.3873	4.4427745	3.9331
All consider parameters but JBE	21.426	3.8663	0.65498
No consider parameters	17.764	3.4789	0.446856

JUPITER BARYCENTER EPHEMERIS UNCERTAINTY

In the previous section we saw that the JBE is the largest source of B-plane uncertainty, which contribute about 165 km in $\mathbf{B} \cdot \mathbf{R}$ direction. However, the expected degree of inflation, as computed by the ephemeris uncertainty associated with DE434, is much less.

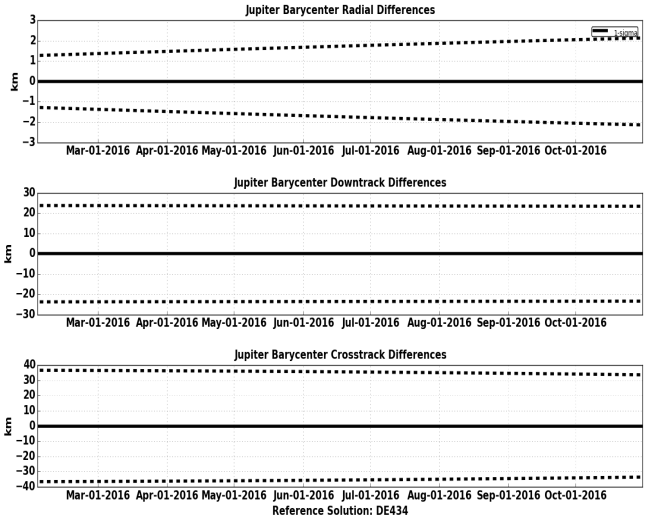

Figure 3. Jupiter barycenter ephemeris uncertainty for DE434. The position uncertainty is dominated by the normal (cross-track) uncertainty with respect to the Sun.

Figure 3 shows the 1-σ position uncertainty of the JBE in dashed lines in the radial-transverse-normal (RTN) frame relative to the Sun. Because of the approach geometry of Juno, the main driver of $\mathbf{B} \cdot \mathbf{R}$ uncertainty is the ephemeris uncertainty in the normal direction. This is clearly observed in Figure 4, where the orbit geometry is shown in EMO2000 frame. The radial uncertainty translates to $\mathbf{B} \cdot \mathbf{T}$, the transverse to TCA, and the normal to $\mathbf{B} \cdot \mathbf{R}$. Thus, from Figure 3, the contribution of the Jupiter barycenter ephemeris uncertainty to the B-plane mapping should be on the order of 1-σ, 40 km to the root sum square (RSS) of the full covariance. Therefore, in Figure 1, the effect of the

uncertainty of the B-plane mapping in $\mathbf{B} \cdot \mathbf{R}$ should not be inflated by a factor > 3 when the JBE is included as a consider parameter. This discrepancy led the OD team to rethink the OD setup and analyze whether the B-plane mapping had been done correctly.

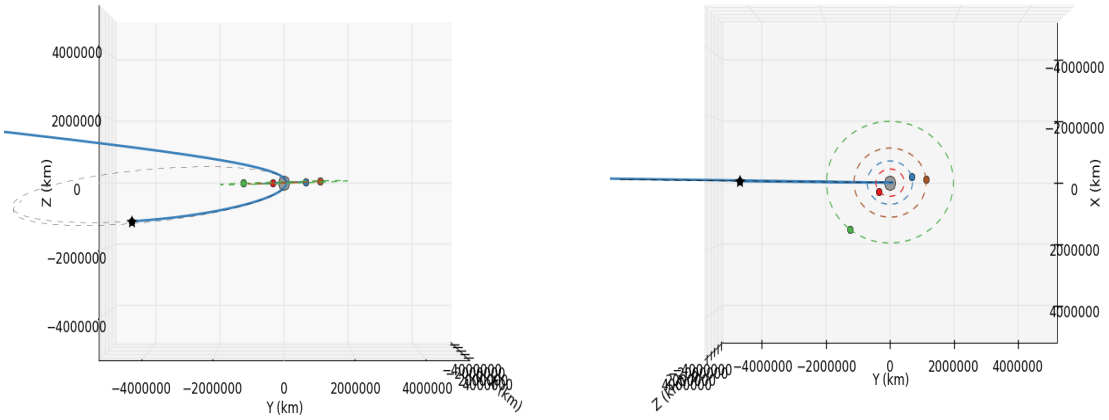

(a) YZ-plane (b) XY-plane

Figure 4. Juno and Jupiter barycenter ephemeris around JOI in EMO2000. The four Galilean moons are also shown. Figure 4(a) is very close to how the Juno orbit appears as viewed from the Earth.

ANALYTICAL SENSITIVITY

The magnitude of the impact vector (B) in Equation 1 is a function of GM, r_p, and V_∞. We noted in the previous section that B primarily lies along $\mathbf{B} \cdot \mathbf{R}$ (Figure 2), and so is its uncertainty as shown in Table 3. Then, ignoring the correlation between the variables, we can write the variance of B as

$$\sigma_B^2 = \left(\frac{\partial B}{\partial GM}\right)^2 \sigma_{GM}^2 + \left(\frac{\partial B}{\partial r_p}\right)^2 \sigma_{r_p}^2 + \left(\frac{\partial B}{\partial V_\infty}\right)^2 \sigma_{V_\infty}^2 \tag{4}$$

Equation 4 is sufficient for a crude, first-order sensitivity analysis. We can compute each term as follows:

$$\frac{\partial B}{\partial GM}\sigma_{GM} = \frac{1}{V_\infty^2\sqrt{1+h}} < 0.01 \text{ km} \tag{5}$$

$$\frac{\partial B}{\partial r_p}\sigma_{r_p} = \frac{1+0.5h}{\sqrt{1+h}} < 5 \text{ km} \tag{6}$$

$$\frac{\partial B}{\partial V_\infty}\sigma_{V_\infty} = -\frac{2GM}{V_\infty^3}\frac{1}{\sqrt{1+h}} < 0.20 \text{ km} \quad (7)$$

where $r_p = 75970\ km$, $\sigma_{r_p} < 1\ km$, $GM = 1.26712764133 \times 10^8\ km^3/s^2$, $\sigma_{GM} < 3\ km^3/s^2$, $V_\infty = 6.0\ km/s$, $\sigma_{V_\infty} < 2 \times 10^{-6}\ km/s$. σ_{r_p} is taken from the RTN frame mapping of Juno with respect to Jupiter at the perijove time (R-component), σ_{GM} is provided by DE434, and V_∞ and σ_{V_∞} are approximated by the velocity uncertainty of Juno of OD139. This back-of-the-envelope calculation yields much lower values for the B-vector uncertainties than the no-consider case in Table 3. Thus, this result indicates that the B-plane mapping uncertainties are inflated even in the absence of the JBE in the consider parameter list.

CURRENT STATE KNOWLEDGE

In this section, we go back to the basics and check if the current state knowledge of Juno, with respect to Jupiter, is properly computed with and without the Jupiter ephemeris in the consider parameter list. For this purpose, we took a solution that has the DCO of 2016-05-19 and applied the mapping immediately after the DCO. To be precise, the DCO is 2016-05-19 05:06:41 ET and the map time is 2016-05-19 11:00:00 ET. These times are roughly seven weeks before perijove. Table 4 presents the RTN position uncertainty of Juno relative to Jupiter with and without JBE in the consider parameter.

Table 4. Current state knowledge of Juno in RTN frame relative to Jupiter on 2016-05-19. The DCO is 2016-05-19 05:06:41 ET and the map time is 2016-05-19 11:00:00 ET.

Parameter	No JBE	With JBE
$\sigma_R\ [km]$	0.83161	22.94283
$\sigma_T\ [km]$	0.82661	35.47445
$\sigma_N\ [km]$	0.24749	3.43964

As shown, the RSS of the position uncertainty grew by roughly $40\ km$ as expected from the position uncertainty of JBE. This result assures that the current time mapping of Juno - Jupiter relative state is done properly. Table 5 compares the B-plane mapping for the same solution with the same DCO and map time.

Table 5. Current state B-plane mapping on 2016-05-19. The DCO is 2016-05-19 05:06:41 ET and the map time is 2016-05-19 11:00:00 ET.

Parameter	No JBE	With JBE
$\sigma_{B\cdot R}\ [km]$	3.2046	39.0696
$\sigma_{B\cdot T}\ [km]$	0.86981	2.6450
$\sigma_{TCA}\ [s]$	0.3003	3.38814

Again, the increase in $\mathbf{B}\cdot\mathbf{R}$ uncertainty is comparable to the normal direction uncertainty in JBE of $40\ km$ and that in TCA is comparable to the tangential direction uncertainty in JBE of $20\ km$ for

a 6 km/s unperturbed flyby. Also, the $\mathbf{B} \cdot \mathbf{R}$ uncertainty is consistent with the analytical calculation in Equations 5 through 7. Thus, we can conclude that the current state mapping is computed properly both with and without JBE for the B-plane, but not when the map time coincides with the perijove. This gave us a clue that the map time is one of the drivers for the covariance inflation.

MAPPING TIMES

The previous analysis indicated that the covariance inflation is influenced by the mapping time. Thus, we tried various map times to keep record of how the B-plane uncertainties change over time. The same OD solution with the DCO of 2016-05-19 is used. This solution incorporates all forces listed in Table 2. Tables 6 and 7 show the B-plane mapping of $\mathbf{B} \cdot \mathbf{R}$ and $\mathbf{B} \cdot \mathbf{T}$ without any consider parameter and with only the JBE in the consider parameter. All other consider parameters are turned off.

Table 6. B-plane mappings without the consider parameters with full dynamics.

Map time [ET]	$\mathbf{B} \cdot \mathbf{R}\ [km]$	$\sigma_{B \cdot R}\ [km]$	$\mathbf{B} \cdot \mathbf{T}\ [km]$	$\sigma_{B \cdot T}\ [km]$
2016-05-19 11:00	-8.21346×10^5	3.2046	-7.8448×10^3	0.8698
2016-07-04 00:00	-8.1707×10^5	3.1944	-4.1052×10^3	2.5342
2016-07-04 23:00	-8.1790×10^5	3.2307	-4.2529×10^3	2.5411
2016-07-05 00:00	-8.2027×10^5	3.3175	-4.2655×10^3	2.5487
2016-07-05 01:00	-8.3167×10^5	4.2086	-4.3254×10^3	2.5830
2016-07-05 02:00	-9.4712×10^5	29.307	-4.9520×10^3	2.9097
2016-07-05 02:48:35	-6.1884×10^5	10.4987	-3.1714×10^3	1.9274
2016-07-05 04:00	-8.6967×10^5	9.6056	-4.5305×10^3	2.7210
2016-07-05 05:00	-8.2643×10^5	3.4085	-4.2895×10^3	2.5768
2016-07-05 06:00	-8.1977×10^5	3.2342	-4.2519×10^3	2.5549

Table 7. B-plane mappings with only JBE in the consider parameter with full dynamics. All other consider parameters are turned off.

Map time [ET]	$\mathbf{B} \cdot \mathbf{R}\ [km]$	$\sigma_{B \cdot R}\ [km]$	$\mathbf{B} \cdot \mathbf{T}\ [km]$	$\sigma_{B \cdot T}\ [km]$
2016-05-19 11:00	-8.21346×10^5	39.0696	-7.8448×10^3	2.645
2016-07-04 00:00	-8.1707×10^5	38.9226	-4.1052×10^3	3.5615
2016-07-04 23:00	-8.1790×10^5	38.7783	-4.2529×10^3	3.5673
2016-07-05 00:00	-8.2027×10^5	38.1067	-4.2655×10^3	3.5825
2016-07-05 01:00	-8.3167×10^5	37.6797	-4.3254×10^3	3.6651
2016-07-05 02:00	-9.4712×10^5	309.765	-4.9520×10^3	4.9613
2016-07-05 02:48:35	-6.1884×10^5	150.582	-3.1714×10^3	2.4951
2016-07-05 04:00	-8.6967×10^5	130.281	-4.5305×10^3	3.6593
2016-07-05 05:00	-8.2643×10^5	47.6443	-4.2895×10^3	3.5916
2016-07-05 06:00	-8.1977×10^5	40.9808	-4.2519×10^3	3.5791

The difference between Tables 6 and 7 are in the uncertainties only, and the means are identical

since they both come from the same solution but with different mapping schemes. The map time of 2016-07-05 02:48:35 ET is the occurrence of the perijove. What is remarkable is the change in the mean value of $\mathbf{B} \cdot \mathbf{R}$ and $\mathbf{B} \cdot \mathbf{T}$, especially $\mathbf{B} \cdot \mathbf{R}$. Its mean value drops by approximately 25 percent in a matter of a few hours, and the associated covariance grows by more than a factor of three with/without the JBE in the consider parameter. This confirms the results of the analytical sensitivity analysis that the covariance inflation occurs even in the absence of the JBE in the consider list. The presence of JBE in the consider parameter list in Figure 2(b) only made the inflation more evident in the B-plane plot. This behavior of the B-plane mapping suggests that the Juno dynamics are highly non-Keplerian during the perijove pass.

To confirm this hypothesis, we removed all Jupiter harmonics (J_2, J_4, and J_6) from the dynamics to see its effect on the B-plane mapping, with no consider parameters (Table 8) and with only the JBE in the consider parameter (Table 9). This effectively makes the Jupiter gravity a point mass. The Galilean moon's gravity and SRP are still active so there is a small degree of perturbation to the otherwise Keplerian dynamics.

Table 8. B-plane mappings without the consider parameters with point-mass Jupiter gravity. There are still perturbations from SRP and Jupiter's satellites.

Map time [ET]	$\mathbf{B} \cdot \mathbf{R}\ [km]$	$\sigma_{B \cdot R}\ [km]$	$\mathbf{B} \cdot \mathbf{T}\ [km]$	$\sigma_{B \cdot T}\ [km]$
2016-05-19 11:00	-8.2134×10^5	3.2046	-7.8447×10^3	0.8698
2016-07-04 00:00	-8.1710×10^5	3.1945	-4.1054×10^3	2.5342
2016-07-04 23:00	-8.1698×10^5	3.1934	-4.2496×10^3	2.5371
2016-07-05 00:00	-8.1701×10^5	3.1933	-4.2506×10^3	2.5373
2016-07-05 01:00	-8.1704×10^5	3.1931	-4.2508×10^3	2.5374
2016-07-05 02:00	-8.1704×10^5	3.1922	-4.2507×10^3	2.5374
2016-07-05 02:48:35	-8.1705×10^5	3.1918	-4.2506×10^3	2.5373
2016-07-05 04:00	-8.1705×10^5	3.1928	-4.2506×10^3	2.5374
2016-07-05 05:00	-8.1705×10^5	3.1931	-4.2508×10^3	2.5374
2016-07-05 06:00	-8.1704×10^5	3.1932	-4.2505×10^3	2.5374

As expected, the mean values of $\mathbf{B} \cdot \mathbf{R}$ and $\mathbf{B} \cdot \mathbf{T}$ remain the same and the difference in the uncertainty in $\mathbf{B} \cdot \mathbf{R}$ is the order that we expect from the JBE normal track uncertainty between the two cases.

EVOLUTION OF V-INFINITY

We have observed in the previous section that the B-plane parameters change rapidly as a function of the map time. In order to study how the B-plane itself is changing, we analyze the changes in V_∞. For that we compute V_∞ with three different Jupiter gravity fields; (1) Jupiter's gravity has all even-degree zonals ($J_2 = 1.46956 \times 10^{-2}$, $J_4 = -5.91313 \times 10^{-4}$, and $J_6 = 2.07751 \times 10^{-5}$), (2) Jupiter's gravity is a point mass, and (3) Jupiter's gravity has all but J_2 zonal harmonics. Note that Jupiter's moons are still present in the dynamics. κ is the angle between the V_∞ vector at the map time and at the perijove map time. We also compare the V_∞ magnitude difference at those epochs. The comparison is made within the same gravity case. Table 10 shows these quantities for different gravity perturbations.

Table 9. B-plane mappings with only JBE in the consider parameter with point-mass Jupiter gravity. There are still perturbations from SRP and Jupiter's satellites. All other consider parameters are turned off.

Map time [ET]	$\mathbf{B} \cdot \mathbf{R}\ [km]$	$\sigma_{B \cdot R}\ [km]$	$\mathbf{B} \cdot \mathbf{T}\ [km]$	$\sigma_{B \cdot T}\ [km]$
2016-05-19 11:00	-8.2134×10^5	39.0696	-7.8447×10^3	2.6450
2016-07-04 00:00	-8.1710×10^5	38.9225	-4.1054×10^3	3.5616
2016-07-04 23:00	-8.1698×10^5	38.9200	-4.2496×10^3	3.5620
2016-07-05 00:00	-8.1701×10^5	38.9247	-4.2506×10^3	3.5607
2016-07-05 01:00	-8.1704×10^5	38.9293	-4.2508×10^3	3.5608
2016-07-05 02:00	-8.1704×10^5	38.9436	-4.2507×10^3	3.5608
2016-07-05 02:48:35	-8.1705×10^5	38.9282	-4.2506×10^3	3.5606
2016-07-05 04:00	-8.1705×10^5	38.9290	-4.2506×10^3	3.5610
2016-07-05 05:00	-8.1705×10^5	38.9472	-4.2508×10^3	3.5607
2016-07-05 06:00	-8.1704×10^5	38.9538	-4.2505×10^3	3.5601

Table 10. Evolution of V_∞ at various mapping times. (1) The full dynamics have J_2, J_4, and J_6 zonal harmonics for Jupiter's gravity. (2) The point-mass removes all those harmonics from the dynamics. (3) No J_2 case removes J_2 but retains J_4 and J_6. κ is the angle between the V_∞ at the map time and at the perijove map time. ΔV_∞ is the difference in the magnitude of V_∞ at those two times. Each gravity case is compared separately.

	(1) Full dynamics		(2) Point-mass		(3) No J_2	
Map time [ET]	$\kappa\ [deg]$	$\Delta V_\infty\ [km/s]$	$\kappa\ [deg]$	$\Delta V_\infty\ [km/s]$	$\kappa\ [deg]$	$\Delta V_\infty\ [km/s]$
2016-05-19 11:00	2.9663	-1.78753	1.3811×10^{-2}	-1.9630×10^{-2}	0.1241	-0.0756
2016-07-04 00:00	2.9548	-1.76841	4.5908×10^{-3}	-5.9191×10^{-4}	0.1130	-0.0565
2016-07-04 23:00	2.9528	-1.77617	2.9296×10^{-4}	2.8897×10^{-4}	0.1115	-0.0556
2016-07-05 00:00	2.9698	-1.79285	4.3104×10^{-4}	1.0251×10^{-5}	0.1116	-0.0559
2016-07-05 01:00	3.0760	-1.86856	5.2987×10^{-4}	-2.1108×10^{-4}	0.1116	-0.0560
2016-07-05 02:00	4.2576	-2.51402	4.0742×10^{-4}	-2.3593×10^{-4}	0.0980	-0.0486
2016-07-05 02:48:35	0.00	0.00	0.00	0.00	0.00	0.00
2016-07-05 04:00	4.5942	-2.10023	6.0349×10^{-4}	-2.9470×10^{-4}	0.0985	-0.0524
2016-07-05 05:00	4.0132	-1.83390	3.1199×10^{-4}	-2.6743×10^{-4}	0.1028	-0.0561
2016-07-05 06:00	3.8957	-1.78914	4.31170×10^{-4}	-1.5032×10^{-4}	0.1025	-0.0561

There is a significant difference in the incoming hyperbolic velocity for each gravity case. Table 10 clearly shows the effects of the zonal harmonics, especially J_2. The point-mass gravity case hardly changes V_∞ as expected except for the contribution from the Jupiter's moons. However, with J_2 in Jupiter's gravity field, $\vec{V}_\infty$, therefore the B-plane itself, changes by nearly 5° and its magnitude $2.5\ km/s$ around perijove. This is a massive perturbation from a gas giant with a close approach geometry. Such strong non-Keplerian dynamics does not occur for other, less massive planets. In fact, the Earth flyby of Juno did not suffer the same problem with the B-plane.[7]

COVARIANCE INFLATION

In the previous section we observed the strong influence of J_2 perturbation on the trajectory. However, we do not yet know if the covariance inflation is occurring because a) the uncertainties at periapsis, in the inertial frame, become large or b) the uncertainties become inflated when the coordinates are transformed from the inertial frame to the B-plane. First, we take a look at the state mapping in EME2000 without the JBE in the consider parameter.

Table 11. State covariance mapping in EME2000 at perijove with point-mass vs full Jupiter gravity. The perijove for the point-mass occurs at 2016-07-05 02:48:35.7510 ET and that for the full gravity at 2016-07-05 02:48:35.7256 ET.

Coordinates	Nominal: point-mass	σ: point-mass	Nominal: full gravity	σ: full gravity
$X\ [km]$	907.317	0.2274	909.076	0.2323
$Y\ [km]$	66736.95	8.2125	66867.68	8.3432
$X\ [km]$	35233.11	15.3746	36032.37	15.3065
$V_x\ [km]$	0.6961	2.1235×10^{-4}	0.7034	2.1086×10^{-4}
$V_y\ [km]$	27.1578	5.8985×10^{-4}	27.5959	5.9082×10^{-3}
$V_z\ [km]$	-51.459	3.0895×10^{-3}	-51.2294	3.1740×10^{-3}

As shown in Table 11, while the coordinates differ significantly, their respective uncertainties do not. Thus, the covariance inflation does not occur for the state mapping to the perijove in the inertial frame. This result is also confirmed with the JBE in the consider parameter but is omitted for brevity. Table 12 compares the B-plane mapping with point-mass Jupiter gravity and full Jupiter gravity at perijove, without any consider parameters. This is a subset of the information presented in Table 6 and 8.

Table 12. B-plane mapping at perijove with point-mass vs full Jupiter gravity with no consider parameters.

Coordinates	Nominal: point-mass	σ: point-mass	Nominal: full gravity	σ: full gravity
$\mathbf{B} \cdot \mathbf{R}\ [km]$	-8.1705×10^5	3.19185	-6.1884×10^5	10.4987
$\mathbf{B} \cdot \mathbf{T}\ [km]$	-4.2506×10^3	2.5373	-3.1714×10^3	1.9274

As shown in Table 12, the zonal harmonics significantly perturb the Juno trajectory to change the B-plane mapping mean values (i.e., the B-plane itself changes, as shown in Table 10, and inflates the covariance). In order to confirm that zonal harmonics are the major player, we compared the point-mass gravity against the gravity that has no J_2 (but retains J_4 and J_6).

We observe that the point-mass gravity and no J_2 gravity are comparable. Table 13 confirms that J_2 is the major source of perturbation. The magnitude of the J_2 acceleration is computed by the following equation:

$$\left|\ddot{\vec{r}}_{J_2}\right| = \frac{3}{2}\frac{GM(R^*)^2}{r^4}J_2\sqrt{5\sin^4\phi - 2\sin^2\phi + 1} \tag{8}$$

Table 13. B-plane mapping at perijove with point-mass vs no J_2 for the Jupiter gravity with no consider parameters.

Coordinates	Nominal: point-mass	σ: point-mass	Nominal: no J_2	σ: no J_2
$\mathbf{B} \cdot \mathbf{R}$ $[km]$	-8.1705×10^5	3.19185	-8.0863×10^5	3.6773
$\mathbf{B} \cdot \mathbf{T}$ $[km]$	-4.2506×10^3	2.5373	-4.2049×10^3	2.5131

where G is the gravitational constant, M is the total mass of the body, R^* is the reference radius of 71492 km, $\vec{r}$ is the spacecraft position in the body frame, and ϕ is the spacecraft latitude in the body frame. For comparison, the perijove occurs around $\phi = 2.81°$ (Figure 5), and the equivalent acceleration on Juno from just J_2 (approximately $0.427\ m/s^2$) at that time is equivalent to Earth's GM pulling the spacecraft at the radius of 30500 km. The monopole acceleration due to the GM of Jupiter is $21.955\ m/s^2$, so the J_2 acceleration is approximately 2% of the monopole.

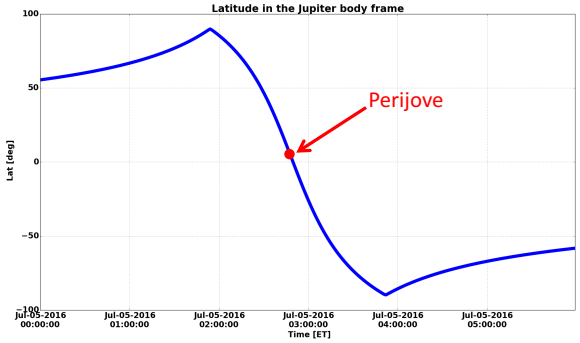

Figure 5. The latitude of Juno in the Jupiter body frame. All times are in ET. The perijove occurs at $2.81°$.

The analysis so far shows that the covariance inflation is occurring between the transformation of the coordinates from the inertial frame (EME2000) to the B-plane. For the uncertainty inflation to occur, because the Juno state uncertainty at DCO is a fixed value, the partial derivative of $\mathbf{B} \cdot \mathbf{R}$ with respect to the Juno state at DCO must become large. Equation 9 shows this partial derivative.

$$\frac{\partial \mathbf{B} \cdot \mathbf{R}}{\partial x_{i,DCO}} = \frac{\partial \mathbf{B} \cdot \mathbf{R}}{\partial \left(r_p, V_\infty, GM\right)} \frac{\partial \left(r_p, V_\infty, GM\right)}{\partial x_{j,map}} \frac{\partial x_{j,map}}{\partial x_{i,DCO}} \tag{9}$$

where x_i and x_j are the dummy variables for the Jupiter-relative position and velocity of Juno. The subscript 'map' and 'DCO' denotes the time of each quantity. The analytical equations in Equations 5 through 7 show that the larger V_∞ results in smaller sensitivity to $\mathbf{B} \cdot \mathbf{R}$. Thus, at perijove, the first component in Equation 9 is actually getting smaller and suggests that the covariance inflation occurs due to other reasons. The second term in Equation 9 is the partial derivative of r_p, V_∞, and GM with respect to the mapped state, and this computation is based on the Keplerian dynamics. The third component in Equation 9 is the state transition matrix (STM) that maps the state from the DCO to the map time with full dynamics, and we have already shown that this STM is similar whether the Jupiter gravity is a point mass or full gravity (Table 11). However, when the partial

derivative with correlations are taken into account, as in Equation 9, the mixed dynamics in the second and third components do not cancel out and in fact they combine to enlarge the uncertainties of GM, r_p, or V_∞. We know that the uncertainty of GM does not change, and the uncertainty of r_p is on the order of a few kilometers (Equation 6). Thus, the inflation must occur because of the inflation in σ_{V_∞}. Table 14 shows the progression of V_∞ at different map times and the associated uncertainty.

Table 14. V_∞ uncertainty over time.

	Full dynamics		Point mass	
Map time [ET]	$V_\infty\ km/s$	$\sigma_{V_\infty}\ km/s$	$V_\infty\ km/s$	$\sigma_{V_\infty}\ km/s$
2016-07-05 00:00	5.3502	2.0767×10^{-6}	5.3752	4.9992×10^{-7}
2016-07-05 01:00	5.2745	1.3412×10^{-5}	5.3750	5.0885×10^{-7}
2016-07-05 02:00	4.6291	1.3977×10^{-4}	5.3750	5.3649×10^{-7}
2016-07-05 02:48:35	7.1431	1.1387×10^{-4}	5.3752	5.2679×10^{-7}
2016-07-05 04:00	5.0429	5.4451×10^{-5}	5.3749	5.1526×10^{-7}
2016-07-05 05:00	5.3092	7.6939×10^{-6}	5.3749	5.2975×10^{-7}
2016-07-05 06:00	5.3540	2.1976×10^{-6}	5.3750	5.3451×10^{-7}

As shown, the uncertainty of V_∞ increases by more than a factor of 50 in only a few hours around perijove. Then, substituting the above uncertainty in the analytical formula given in Equation 4, the expected covariance is on the order of $10.5\ km$ in $\mathbf{B} \cdot \mathbf{R}$. This number is in line with Table 6 and proves that it is the inflation in V_∞ uncertainty that triggered the overall B-plane mapping inflation. The shortcoming of the analytical approach was due to the approximation of V_∞ by the current state knowledge at the time of DCO.

NEW B-PLANE MAPPING

We have confirmed that J_2 perturbation is the major culprit for the inflated covariance in the B-plane. The dynamics of Juno becomes highly non-Keplerian and the partial of V_∞ grows rapidly around perijove. After the source of the problem was identified, we changed the map time from the event mapping of perijove (old) to a fixed time of 2016-07-04 00:00:00 ET (new). Figure 6 shows the old and new B-plane mappings, and compares the behavior of the covariance between the no consider parameter case, no JBE consider parameter case, and all consider parameter case.

In Figure 6(a), the importance of the map time for the B-plane mapping is evident. For the B-plane to be valid, the dynamics at the map time needs to be sufficiently close to the two-body dynamics assumed for its construction. When this two-body assumption is violated, the B-plane mapping does not agree with our expectation. Figure 6(b) shows the B-plane mapping with the new map time for different consider parameter cases. The green is the no consider case, which only depends on the dynamics (position and velocity) of Juno, the red is the full consider case, and the blue ellipse removes the JBE from the consider list but retains all others. The difference between the blue and red ellipses are on the order of the $40\ km$ we expect from the normal track uncertainty of JBE, and TCA uncertainty roughly $4\ s$ (roughly $22\ km$ uncertainty in transverse direction for $5.3\ km/s$ hyperbolic velocity as shown in Table 14). The comparison of the uncertainties in Figure 6(b) are presented in Table 15.

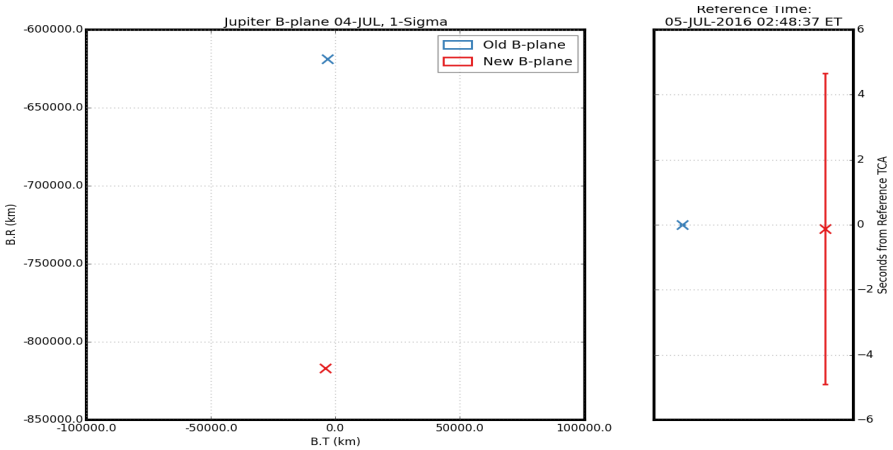

(a) Old and new B-plane mappings.

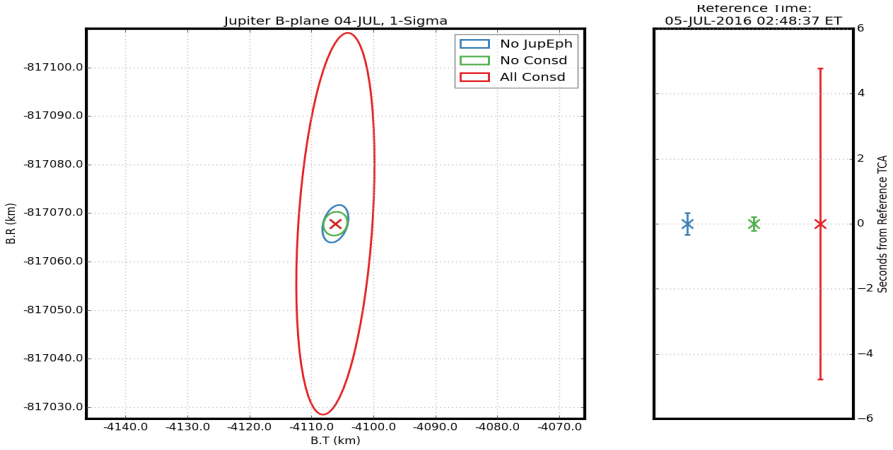

(b) New B-plane mapping with and without consider parameters.

Figure 6. Old and new B-plane mappings. On the top figure, the old B-plane mapping is only shown as a target without a covariance associated with it.

Table 15. B-plane mapping uncertainties with the new mapping time.

Case	$\sigma_{B\cdot R}\ [km]$	$\sigma_{B\cdot T}\ [km]$	$\sigma_{TCA}\ [s]$
All consider parameters	39.324	6.306	4.751
All consider parameters but JBE	3.868	2.097	0.389
No consider parameters	2.446	1.945	0.222

CONCLUSION

This manuscript discussed the B-plane mapping of Juno during the approach phase and its behavior associated with an unexpected covariance inflation. This work was triggered when we realized that the magnitude of the covariances between the cases that do and do not consider the Jupiter barycenter ephemeris did not match our intuition. Specifically, the uncertainty of $\mathbf{B} \cdot \mathbf{R}$ is directly

correlated with the normal track uncertainty of the Jupiter barycenter ephemeris, which is roughly $40\ km$. Our expectation is that for the case that considers the Jupiter barycenter ephemeris, $\sigma_{B\cdot R}$ should be about $40\ km$ larger than if we did not consider it (the state uncertainty is much smaller). Instead, the covariance was inflated by more than $140\ km$, larger than a three-fold increase in $\sigma_{B\cdot R}$.

First we looked at the analytical B-plane parameter sensitivity analysis. This first-order calculation shows that the covariance inflates more than our expectation, even if we do not include JBE in the consider parameter. Then we checked Juno's heliocentric state uncertainty with and without the JBE as a consider parameter, at the time of data cutoff. We showed that the uncertainty of the Jupiter barycenter ephemeris was properly accounted for in the relative state uncertainty of Juno and Jupiter. Interestingly, the B-plane mapping at the data cutoff also properly accounts for the JBE uncertainty in $\sigma_{B\cdot R}$ to meet our expectation. Subsequent analysis identified that the map time shows great sensitivity to the B-plane mapping time due to Jupiter's strong perturbations from the zonal harmonics. Although the construction of the B-plane assumes Keplerian dynamics, the actual Juno dynamics were significantly perturbed. This is one important and unique lesson we learned for a very close spacecraft approach to a gas giant.

Further analysis shows that J_2 zonal coefficient is the most influential parameter, and in fact, its effect is so strong that V_∞ changes by more than $2.5\ km/s$ in a matter of less than one hour around perijove. As a result, the incoming approach angle changes by more than 4°. After the problem and its cause were identified, we proceeded to change the map time from perijove event time to a fixed time of 2016-07-04 00:00:00 ET. This change resulted in a more consistent behavior of the B-plane mapping with our expectation that accounts for the spacecraft state uncertainty and the JBE uncertainty.

Juno is currently in 53-day orbit and collecting science data during perijove passes.

ACKNOWLEDGMENT

This work was supported by the Juno project and conducted at the Jet Propulsion Laboratory, California Institute of Technology under a contract with NASA.

REFERENCES

[1] W. Kizner, "A Method of Describing Miss Distances for Lunar and Interplanetary Trajectories," *Planetary and Space Science*, Vol. 7, 1961, pp. 125–131.

[2] D. Farnocchia, S. R. Chesley, A. Milani, G. F. Gronchi, and P. W. Chodas, *Orbits, Long-term Predictions, Impact Monitoring*. University of Arizona Press, 2015.

[3] B. D. Tapley, B. E. Schutz, and G. H. Born, *Statistical Orbit Determination*. Elsevier Academic Press, 2004.

[4] G. J. Bierman, *Factorized Methods for Discrete Sequential Estimation*. Academic Press, 1977.

[5] P. F. Thompson, S. Ardalan, J. Bordi, N. Bradley, D. Farnocchia, and Y. Takahashi, "Juno Navigation for Jupiter Orbit Insertion," *27th AAS/AIAA Spaceflight Mechanics Meeting, San Antonio, Texas*, No. 17-459, 2017.

[6] R. Park, W. M. Folkner, and R. A. Jacobson, "The Planetary Ephemeris DE434, IOM 392R-15-018," *JPL Inter-Office Memorandum*, 2015.

[7] P. F. Thompson, M. Abrahamson, S. Ardalan, and J. Bordi, "Reconstruction of Earth Flyby by the Juno Spacecraft," *24th AAS/AIAA Spaceflight Mechanics Meeting, Santa Fe, New Mexico*, No. 14-435, 2014.